

Analog and Digital RoF Spatial Mux MIMO-LTE System based A² (arithmetic Aquila) optimization model for 5G network

Irfan Ahmad Rather¹, Gulshan Kumar¹, Rahul Saha¹

¹ School of Computer Science and Engineering, Lovely Professional University, Phagwara, Punjab, India.

Abstract

Multiple input multiple output-long term evolution (MIMO-LTE) with radio over fiber (RoF) link is an emerging technology for the next generation wireless network including 5G. In next generation (NG) network requires huge data rates to transmit the data in a wireless channel. Thus, efficient transmission and high data rate is considered as the essential requirement in MIMO system. Hence, RoF technology is introduced to improve the reliability of the 5G wireless communication (WC). In this research, each antenna deals with 800 MHz 5G signal (totally 3.2GHz) having 64 bit quadrature amplitude modulation (QAM). In addition to this, a 70Km of standard single mode fibre (SSMF) is introduced for broadband wireless signal transportation and distributed applications. Moreover, utilization of band pass sampling takes place and defined the model to degrade the bandwidth requirement in RoF link. The performance is analysed for both digital RoF (D-RoF) and conventional analog RoF (A-RoF)). The optimal transmission condition of the RoF fronthaul system in MIMO system is also analysed. To optimize the transmission condition of the link RoF, the bias current and power transmission is optimized using arithmetic Aquila optimization strategy. The entire work is implemented in MATLAB tool. The performance measures such as and eye opening penalty (EOP), error vector magnitude (EVM) and signal to noise ratio (SNR) are analysed for both D-RoF and A-RoF systems. In experimental scenario, the D-RoF and A-RoF has the EVM of 1.45% and 1.13%, EOP of 51.19dB and 51dB, SNR of 27dB and 26dB, computation time of 0.14s are attained. The experimental analysis is compared with existing techniques such as Aquila optimizer (AO), chimp optimization (CO), remora optimization (RO) and particle swarm optimization algorithm to prove the efficiency of the proposed method.

Keywords

MIMO-LTE, RoF link, 5G network, arithmetic Aquila optimization, band pass sampling, EVM

1. Introduction

The MIMO technology play an important role in 4G long term evolution (LTE) systems to achieve high data rates in both uplink and downlink channels [1]. The MIMO-LTE system uses multiple antenna at the transmitter and receiver side to enhance the capacity of the system [2]. In addition, the MIMO system prevents the high usage of bandwidth and power compared to SISO communication systems [3]. In MIMO-LTE system, cloud radio access network (C-RAN) is highly recommended to increase the capacity of the system [4]. The C-RAN system works based on the baseband unit (BBU) with different standards of the processing signals [5]. Generally, MIMO-LTE systems uses RoF links to enhance the connection between BBU and remote radio heads (RRH) [6].

The MIMO-LTE with RoF links uses very high broad bandwidth with low power loss as they are highly suffered due to some non-linear distortions [7]. However, these distortions are due to fiber dispersion as well as the electrical to optical and optical to electrical conversions [8]. This drawback

ACM-2022: Algorithms Computing and Mathematics Conference, August 29 – 30, 2022, Chennai, India.

EMAIL: rsahaot@gmail.com (Rahul Saha)

ORCID: 0000-0003-3921-9512 (Rahul Saha)

 © 2022 Copyright for this paper by its authors.

Use permitted under Creative Commons License Attribution 4.0 International (CC BY 4.0).

 CEUR Workshop Proceedings (CEUR-WS.org)

leads to failure in spectrum re-development and it is said to be adjacent channel interference (ACI) [9]. Now-a-days, the usage of OFDM based LTE or LTE-A systems provides major advancements in overcoming the wireless channel distortions [10]. But it is highly prone to distortion because of high peak to signal noise ratio (PAPR) during signal addressing. Recently, there are many studies undertaken to understand the MIMO-LTE systems performance that pays more attention to the transceiver signals [11].

Commonly, some of the quadrature phase imbalance (I/Q) may occur in space time diversity systems [12]. This can be analyzed at the prior stage without the use of non-linearity in the transmitter section. Before data transmission, some of the typical crosstalk arises and it must be deeply analyzed using MIMO schemes [13]. Using couplers in the RF transmitter, the crosstalk is continuously analyzed without the use of real framework of the MIMO schemes. Generally, the data transmission in MIMO system takes place with the same local oscillator (LO) thus the power consumption is highly reduced. In MIMO RoF systems, double sideband frequency translation (DSB-FT) and single sideband frequency translation (SSSB) approach is used for cost reduction [14]. This approach works based on the principle of two MIMO channels that utilizes same LO. In SSB frequency translation system, filtering technique is introduced to prevent the loss of power in the LSBs and USBs [15].

The recent trend in 5G wireless communication proves that integration of several communication structures, vehicular proximities and switching techniques has become more important. The MIMO techniques enhances the communication performance by enhancing the speed of transmission, bit rate, and capacity of the channel. MIMO usually takes multipath propagation by enabling various antennas in the transmitter and receiver side. However, the 5G technology had been emerged in late 2020 and it mainly enhances the capacity and spectral efficiency of the MIMO-LTE systems. In order to enhance the signal performance and fast transmission, MIMO is introduced into the LTE system. In traditional coaxial cable, high data losses may arise and the best solution is the introduction of RoF link in the MIMO-LTE systems. Furthermore, the presence of optical fiber produces broad bandwidth and immunity to electromagnetic interference. Only minor researches had been undertaken for improving the transmission capacity of MIMO-LTE RoF link. But these technique lacks to provide the transmission capacity in the MIMO system. Hence, an effective approach is required to enhance the transmission capacity of the MIMO-LTE system. These kinds of major drawbacks motivate us to develop an enhanced approach for improving the transmission capacity of the MIMO-LTE systems. In this research, the 4×4 MIMO LTE 5G signal of about 3.2 GHz with 64-QAM over 70Km of SSMF is introduced to transmit the data in distributed applications. In addition, band pass sampling is emphasized to reduce the overall requirement of bandwidth (BW) in the RoF link. In order to enhance the transmission condition, bias current and the power transmission is optimized using A^2 optimization approach. The major contribution of the proposed work is clearly depicted below:

- This research mainly aims to enhance the transmission condition of the RoF Spatial Mux MIMO-LTE System.
- A 4×4 MIMO LTE system with 3.2GHz 5G signal having 64-QAM over 70Km of SSMF is introduced to enhance the transmission condition of the system.
- To reduce the BW requirement, band pass sampling is performed in the RoF link.
- To analyze the performance based on conventional A-RoF and D-RoF.
- For optimizing bias current and power transmission, A^2 optimization strategy is emphasized in the proposed approach.
- The performance of the proposed method is analysed using MATLAB software tool.
- The performance measures such as EVM, SNR and EOP are analyzed for both D-RoF and A-RoF systems.

The rest of the paper is organized in the following manner. Literature survey is described in section 2. The MIMO system model is discussed in Section 3. Proposed method is explained in Section 4. More precisely, it explains the optimization algorithm used in this work. In Sections 5 and 6, the simulation results and conclusion are provided, respectively.

2. Literature Survey

Carlos et al. [16] had defined the evaluation of non-linear effects in a RoF Spatial Mux MIMO-LTE Fronthaul system. This method mainly helps examine the RoF link's transmission quality for the MIMO system. By altering the laser bias current and the input signal power, the transmission circumstances can be minimized in RoF fronthaul system. The carrier frequency was set to 2.65GHz with the band 7 in LTE standard. The bias current was properly evaluated by reducing the ACPR and the EVM. In the experimental scenario, the ACPR attained was about -43.7 for the bias current of 25mA in QPSK modulation. However, this method suffered from high attenuation in the MIMO RoF link.

Mateo et al. [17] studied the RoF spatialMux MIMO-LTE fronthaul system for transmission parameter selection using optimization algorithm. In this method, nelder-mead optimization algorithm was introduced to overcome the transmission circumstances in the MIMO system. This algorithm helps optimize the signal power and the bias current in the lasers for varying iterations. The experiment was carried out via the MIMO IMD RoF system, in which each MIMO signal was multiplexed. The signals and the carrier frequency were estimated based on the LTE property. The maximum EVM attained about 1.85% in the experimental scenario for 11 iterations in QPSK modulation. However, this method suffered due to high SNR and interference.

Hafez et al. [18] had defined the transmit diversity and spatial multiplexing MIMO techniques in LTE cell edge coverage areas. In this method, the working of transmit antenna diversity and spatial multiplexing for the proposed MIMO-LTE system is clearly explained. Separate analysis have been undertaken for both 2×2 and 4×4 MIMO-LTE systems. To analyse the performance of the MIMO system, MATLAB tool was used. In experimental scenario, the throughput of 100% was obtained for the SNR of -5dB. However, this method was suffered due to high data loss and poor spectral efficiency.

Kanesan et al. [19] investigated an alternative system to 2×2 MIMO for LTE over 60Km RoF link. In this method, QPSK, 16 bit QAM and 64 bit QAM was manipulated as single carrier frequency (SCM) based on LTE standard. This technique can be modulated by introducing FDM into the orthogonal FDM. In order to prevent data losses in the MIMO system, 60km RoF link was introduced. In experimental scenario, the EVM attained about 5.8%, 5.9% and 5.97% for QPSK, 16-QAM, 64-QAM system. However, this method shows low capacity when the density of the user gets increased.

Kim et al. [20] had introduced MIMO RoF system and its applications in mm wave-based indoor 5G WCs. In this method, RoF based distributed antenna system (DAS) was experimentally carried out using OTA interface on the 4 basis of broadband 5G signal. For MIMO system modulation, 256-bit QAM was utilized. The MIMO based 5G system was in cooperated with the mm wave-based Korea telecom (KT) for achieving high throughput. In experimental scenario, the EVM attained about 4% for 2Km RoF link. However, this method was suffered due to high transmission delay and computational complexity.

2.1. Problem Formulation

From the deep analysis of the aforementioned related works, the existing techniques are highly suffered due to major drawbacks such as high transmission circumstance, computational complexity, channel fading etc. In [16], ROF spatial Mux MIMO-LTE Fronthaul system transmission parameter selection with optimization algorithm was introduced by the author. But this method was badly affected due to channel fading because of high interference. In [17], evaluation of non-linear effects in a RoF Spatial Mux MIMO-LTE Fronthaul system was defined by the author. This system causes high fluctuation when the bias current increases. In [18], the author introduced the performance analysis of transmit diversity and spatial multiplexing MIMO techniques in LTE cell edge coverage areas. Even though advanced technique was introduced this method affected due to high power consumption and time complexity. In [19], the author defined the theoretical and experimental design of an alternative system to 2×2 MIMO for LTE over 60Km RoF link. But this method was limited due to high data loss and produces low performance quality. In [20], MIMO-supporting RoF system and its applications in

mm wave-based indoor 5G mobile network was introduced by the author. But these techniques high EVM which are practically not suitable in real time applications.

3. Analog and Digital RoF Spatial Mux MIMO-LTE System model

In WC system, the data rates can be enhanced by increasing the signal power received in the communication link. However, the signal power received can be increased by introducing MIMO system into the WCs. Some of the present standards like LTE or LTE-A are mainly responsible for maximizing the rate of data. In system like LTE, each antenna develops the resource grid by generating and transmitting the OFDM symbols and signals respectively. The data rates can be improved by extending the multiple antenna with the rid of modes in the MIMO system.

There are four types of transmission modes in the LTE standards namely receiver combination, spatialMux, TxDiversity, and beamforming. In spatialMux, the system transmits the signal independently on different antennas. In TxDiversity, the redundant data is transmitted on various antenna without increasing the data rate. The spatialMux mode have the ability to enhance the data rate and it is directly proportional to the number of transmit antennas. Moreover, the layer mapping operation is performed that converts the data into layers. This operation is done until the layer de-mapping which is same as the single MIMO antenna. After, demodulation process MIMO system undergoes pair of operations. If any one of the signal gets distorted, other signals also gets affected during demodulation process.

4. Proposed methodology

In 5G communication system, huge data rates are required to transmit the data in MIMO-LTE system. As a result, more transmission circumstances arises in the MIMO RoF system. Hence, this research mainly aims to enhance the transmission condition of the RoF Spatial Mux MIMO-LTE System. A 4×4 MIMO LTE system with 3.2GHz 5G signal having 64-QAM over 70Km of SSMF is introduced for signal transmission. Moreover, band pass sampling is emphasized to reduce the overall BW requirement in the RoF link. In order to find the best value for transmission condition, bias current and transmitted power need to be optimized. Here, A^2 optimization strategy is introduced to optimize the bias current and transmitted power. The performances are analysed under A-RoF and D-RoF using MATLAB tool.

4.1. Hybrid A^2 Algorithm

During exploration phase, the individual AO swarm perform fast flight and hunting in the search space. According to the global best solution, position of individual gets updated and that leads to greater convergence and strong searching capability. However, the individual has low capability of escaping from the local optima. Hence, the individual gets easily trapped into the local optima. In experimental scenario, the multiplication and division operator in the exploration stage is too low and thus results in insufficient population diversity. Moreover, the switching mechanism for both exploration and exploitation phase is not good and to overcome this AO and AOA algorithm needs to be hybridized.

Based on the four predation stages, the prey is caught by each AO swarms.

First stage: In this stage, the Aquila will fly in the hunting location with the high altitude. This helps to search the food and find the target more efficiently. After the prey is found, it with fly vertically to catch the prey and its behaviour is mathematically formulated as,

$$Y(s+1) = Y_{best}(s) * (1 - \frac{s}{S}) + (Y_N(s) - Y_{best}(s) * rand) \quad (13)$$

Here, $Y(s+1)$ indicates the individual position at $(s+1)$ iteration, $Y_{best}(s)$ indicates the present global best solution at $s-th$ iteration. Also, s and S demonstrates the present $s-th$ iteration and the maximum iteration count, $(Y_N(s))$ indicates the average position of current individual during present iteration and $rand$ represents the random Gaussian distribution between the interval 0 and 1.

Second stage: In this stage, the Aquila will divert its flying from high altitude to levitate its prey head. This helps to prepare the Aquila to instinct the predation behaviour. The updated position is mathematically formulated as,

$$Y(s+1) = Y_{best}(s) * LF(W) + Y_r(s) + (v - u) * rand \quad (14)$$

Here, $Y_r(s)$ indicates the Aquila's random position, W indicates the width size, LF indicates the levy flight function, v and u indicates the search shape and it is mathematically formulated as,

$$\begin{cases} u = (n_1 + 0.0056 * W_1) * \sin(-\lambda * W_1 + \frac{3\pi}{2}) \\ v = (n_1 + 0.0056 * W_1) * \cos(-\lambda * W_1 + \frac{3\pi}{2}) \end{cases} \quad (15)$$

$$LF(u) = 0.001 * \frac{\alpha\beta}{|\omega|^\mu}, \beta = \left(\frac{\left(\Gamma(1 + \mu) * \sin\left(\frac{\mu\pi}{2}\right) \right)}{\left(\Gamma\left(\frac{1+\mu}{2}\right) * \mu * 2^{\left(\frac{\mu-1}{2}\right)} \right)} \right)^{\frac{1}{\mu}} \quad (16)$$

Here, n_1 indicates the number of search cycles starting from 1 to 20, W_1 represents the random integer starting from 1 to width W and λ represents the constant that have the value of 0.005.

Third stage: In this stage, the Aquila begin to discover and establish an approximate prey's location. Then, the Aquila will decline vertically for primary predation to reduce the speed of the prey. The mathematical expression for initial predation behaviour is given as,

$$Y(s+1) = (Y_{best}(s) - Y_N(s)) * \phi - rand + ((UL - LL) * rand + LL) * \mathcal{G} \quad (18)$$

Here, ϕ and \mathcal{G} indicates the adjustment parameters with the fixed value of 0.1, UL and LL demonstrates the upper and lower limit of the searching space respectively.

Final stage: In this stage, the Aquila reaches the land area to follow the prey to chase and attack the prey. The predation behaviour of the Aquila is mathematically formulated as,

$$Y(s+1) = (QF * Y_{best}(s) - (M_1 * Y(s) * rand) - M_2 * LF(W) + rand * M_1 \quad (19)$$

$$QF(s) = s^{\frac{2rand-1}{(1-s)^2}} \quad (20)$$

$$\begin{cases} M_1 = 2rand - 1 \\ M_2 = 2 \times \left(1 - \frac{s}{S} \right) \end{cases} \quad (21)$$

Here, QF represents the quality function of the search strategy, M_1 denotes the random movement of tracking the Aquila's prey under the range $[-1,1]$ and M_2 indicates the gradient flight for tracking Aquila's prey.

The AOA algorithm is introduced to optimize the exploration and exploitation phase using four arithmetic operations.

In exploration phase, the arithmetic operators such as division and multiplication operation are used to generate highly distributed values. It is more accurate and hence the highly distributed values does satisfy to reach the target easily. The main property of these two operators are highly recommended for the search space. It can be mathematically formulated as,

$$Y(s+1) = \begin{cases} Y_{best}(s) \div (mop + \gamma) * ((UL - LL) * \rho + LL) & \text{if } r_2 < 0.5 \\ Y_{best}(s) * mop * ((UL - LL) * \rho + LL) & \text{otherwise} \end{cases} \quad (22)$$

$$\left\{ \begin{array}{l} mop(s) = 1 - \frac{s^{\frac{1}{\sigma}}}{S^{\frac{1}{\sigma}}} \\ moa(s) = \min + s * \left(\frac{\max - \min}{S} \right) \end{array} \right. \quad (23)$$

Here, γ denotes the compact integer and ρ manipulates the control parameter for search process and it have the fixed value of 0.5. Also, mop indicates the math optimizer probability, σ indicates the sensitive coefficient that helps to represent the development accuracy with the fixed value of 5, moa indicates the math optimizer acceleration that helps to choose the search space, \max and \min indicates the maximum and minimum values for acceleration function.

In the second stage, high density results are generated with the aid of subtraction and addition operations. These two operators have less dispersion and are easy to reach the destination place. Hence, these operators are emphasized into the exploration stage and it is mathematically formulated as,

$$Y(s+1) = \begin{cases} Y_{best}(s) - mop * ((UL - LL) * \rho + LL) & \text{if } r_3 < 0.5 \\ Y_{best}(s) + mop * ((UL - LL) * \rho + LL) & \text{otherwise} \end{cases} \quad (24)$$

The hybrid A^2 algorithm gives the optimum transmission circumstances in the environment of the assessed system, which satisfy $\arg \min EVM(I_{bias1}, I_{bias2}, P_{in})$. The input signal power (P_{in}) is set between -35 and -20 dBm, and both branches bias currents (I_{bias1} and I_{bias2}) are set between 20 and 80 mA in order to avoid the threshold limit and the saturation region.

$$Fitnessvalue = \arg \min EVM(I_{bias1}, I_{bias2}, P_{in}) \quad (25)$$

Let us assume the difference for equation (13), (14), (21) and (23), the individuals of AO swarms would process more random search than individual of AOA swarms. The mathematical calculations for the exploitation phase is presented in the equation (17), (18), (21) and (23), the individual of AO swarm works worse compared to individuals of AOA swarms. The exploitation capacity of the individual AOA swarms are low compared to individuals in AO swarms. It would be better when the individuals of AO swarms in the exploration phase is hybrid with individuals of AOA swarms in the exploitation phase. Figure (1) illustrates the flowchart of A^2 algorithm

Pseudo code for hybrid A^2 algorithm
Step 1: Set population size M
Step 2: Set the maximum number of iteration as S
Step 3: Set width as W
Step 4: Initialize the individual position as $Y_x (x = 1, 2, \dots, M)$

```

While ( $s \leq S$ )
Update  $mop$  and  $moa$  with the aid of Equation (13)
Update ,  $v$  and  $u$  with the aid of Equation (15)
Step 5: For  $x = 1 : M$ 
If  $|\varepsilon| \geq 1$ 
Step 6: If  $rand < 0.5$ 
Update position of  $Y(s+1)$  with the aid of Equation (13)
Else
Update position of  $Y(s+1)$  with the aid of Equation (14)
End if
Step 7: If  $rand < moa$ 
If  $rand < 0.5$ 
Update position of  $Y(s+1)$  with the aid of Equation (21)
Else
Update position of  $Y(s+1)$  with the aid of Equation (21)
End if
Step 8: Else
If  $rand < 0.5$ 
Update position of  $Y(s+1)$  with the aid of Equation (23)
Else
Update position of  $Y(s+1)$  with the aid of Equation (23)
End if
End if
Else if
Step 9: End for
For  $x = 1 : M$ 
Check if the position reach out of search space limit and
return back
Calculate the fitness of  $Y(s)$ 
Update  $Y_{best}(s)$ 
Step 10: End For
 $s = S + 1$ 
Step 11: End while
Return  $Y_{best}(s)$ 

```

4.2. Utilization of band pass sampling

The sampling Nyquist/Shannon always needs a greater sampling frequency to digitalize the modulated RF signal having carrier frequency F_c , bandwidth BW and with the GHz range. To achieve this, high speed electronics need to be operated at least for twice as $(F_c + BW/2)$ Hz. the symbol rate is set to 16 Msymbols/s and the carrier frequency F_c at 2.475 with 3.2 GHz of BW. For band pass sampling, the sampling frequency F_s need to assure the following condition to avoid spectral aliasing among the RF signals

$$2 \frac{F_{\max}}{M} \leq F_s \leq 2 \frac{F_{\min}}{M-1} \quad (26)$$

$$1 \leq M \leq f_f \left[\frac{F_m}{F_{\max} - F_{\min}} \right] \quad (27)$$

Here, F_{\max} represents the maximum frequency and F_{\min} indicates the minimum frequency in which the band is sampled, M indicates the integer, $F_{\max} - F_{\min}$ denotes the band pass signal BW, f_f indicates the floor function that produces the upper rounding to integer of the ratio $\left\lceil \frac{F_m}{F_{\max} - F_{\min}} \right\rceil$. In band pass sampling, many duplicate band pass signal are generated. Hence, a long guard band of 13 MHz is placed on both sides of the central frequency to eliminate the spectral aliasing. Mostly, the spectral aliasing happens due to critical band pass sampling and the entire channel BW attains 46MHz. Hence, the practical values are considered as the 2.49GHz and 2.45GHz for F_{\max} and F_{\min} respectively. The critical sampling frequency is obtained as $2 * 46 = 92 \text{ MSa/s}$. From the equation (2), M can utilize the integer value from 1 to 54. Consider M as 2, the sampling frequency F_s attains the value of 24.95 MSa/s which is greater than critical sampling. Considering the 8 bit ADC that has low cost and low power, the bit rate generated about 1.024Gbps.

4.3. D-RoF analytical model

The D-RoF link model has been recognized using VPI transmission approach. A 64 bit signal called QAM RF is given into the ADC having m number of bits that performs digitalization using band pass sampling technique. In addition to this, quantization and coding operation also takes place in this section. In quantization, continuous signal gets discretised based on ADC resolution in discrete time and amplitude domain. Figure (1) illustrates the systematic block diagram of proposed method

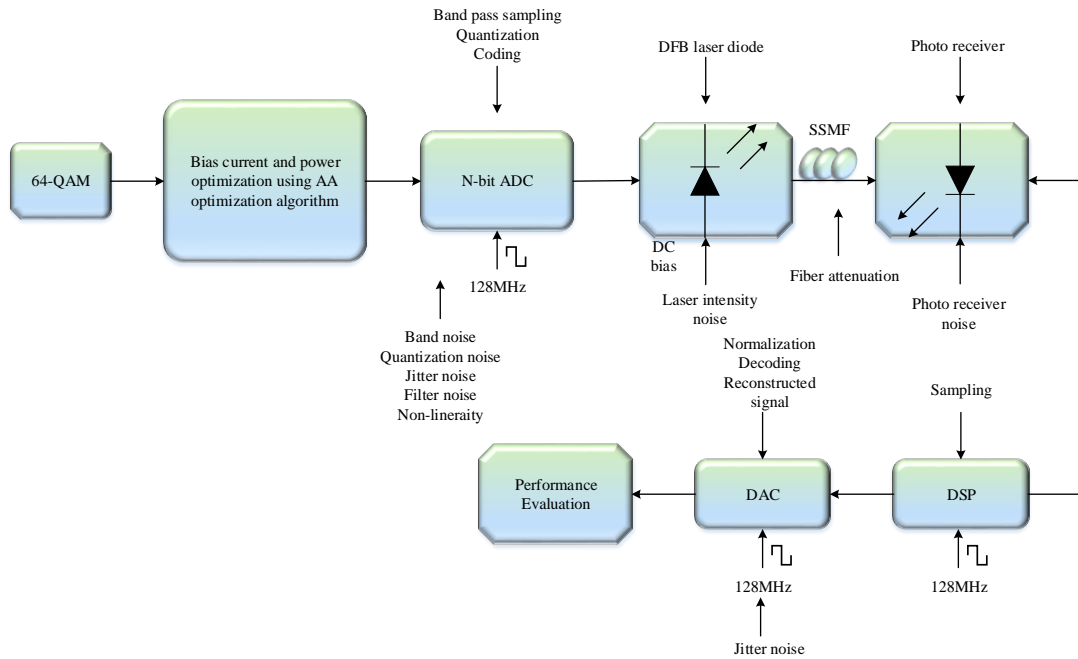


Figure 1: Systematic block diagram of proposed method

After quantization, the signal is converted into binary sequence and encoded using miller encoder. The outcome signal helps to modulate the distributed feedback (DFB) laser diode. In this section, the electrical signal is converted into optical signal. The generated optical signal is then transmitted through optical channel of SSMF. The transmitted signal is then detected using photo-receiver with the rid of PIN photo-detector. The final outcome signal is then fed into the digital signal processor (DSP) and the optical signal is converted into digital signal. The digitalized signal is then fed in to DAC to perform

normalization, decoding and signal reconstruction operations. The reconstructed signal is then fed in to performance evaluator block to analyse the performance of SNR, EVM and EOP.

When the band pass signal is resampled from the band noise gets handled using Nyquist region. In addition to this, the ADC also produces jitter and quantization noise into the RoF link. The quantization noises are generated due to resolution of bits in the ADC. Moreover, the jitter noise occur within the ADC itself and at the sampling clock. In the receiver side, the DAC are highly subjected to jitter noise and this mainly caused due to phase noise of the clock.

Due to band pass sampling, signal degradation, clock jitter noise and quantization noise are generated. The generated noise sources are considered as independent due to weak correlation of the RoF link. The average of band pass sampling, jitter and quantization noises are null. The clock jitter produced in DAC jitter noise are also assumed as independent for both optical link and ADC.

The SNR for the ADC jitter noise is mathematically manipulated as,

$$SNR_{jitter\ ADC} (dB) = -20 \log_{10} (2\pi F_c \mu_{ADC\ jitter}) \quad (28)$$

Here, $F_c = 2.4\ GHz$; $\mu_{jitter} = 0.8\ ps$; whereas μ_{jitter} manipulates the ADC RMS jitter.

The SNR for the ADC quantization noise is mathematically formulated as,

$$SNR_{quantization} (dB) = -20 \log_{10} ((PAPR) + 6.02m + 10 \log_{10} (3)) \quad (29)$$

Here, $PAPR = \frac{3(\sqrt{N} - 1)}{(\sqrt{N} + 1)}$; $N = 64$; $m = \text{Number of bits}$.

The SNR for the band noise aliasing is mathematically expressed as,

$$SNR_{band\ noise\ aliasing} (dB) = \frac{2P_o}{MF_s KT} \quad (30)$$

Here, P_o indicates the output power of modulated RF signal, M indicates the integer of Nyquist region, F_s indicates the sampling frequency, K represents the Boltzmann constant, T manipulates the kelvin temperature.

In DAC, the signal degradation arises due to jitter noise and it can be mathematically manipulated as,

$$SNR_{jitter\ DAC} (dB) = -20 \log_{10} (2\pi F_c \mu_{DAC\ jitter})^{-2} \left[\sin c \left(\frac{F_c}{F_s} \right) \right]^{-2} \quad (31)$$

Here, $F_c = 2.4\ GHz$; $\mu_{jitter} = 0.8\ ps$ and $F_s = 128\ MHz$.

The ADC resolution should be aware that quantization noise is distributed uniformly. This shows that SNR of quantization noise is greater than SNR of jitter noise.

$$SNR_{quantization} > SNR_{jitter} \quad (32)$$

The above equation can be expanded as,

$$-20 \log_{10} ((PAPR) + 6.02m + 10 \log_{10} (3)) > -20 \log_{10} (2\pi F_c \mu_{jitter}) \quad (33)$$

Here, $PAPR$ indicates the peak to average power ratio and it attains the value of 8.1dB, $F_c = 2.4 \text{ GHz}$; $\mu_{jitter} = 0.8 \text{ ps}$. Here, $m = 8$ is chosen for the optimal solution of the ADC.

Some of the non-linearity causes ADC to degrade its operation. Therefore, the ADC needs to be composed with the ideal device along with the integration of different noise. Thus, the distortion can be reduced by introducing non-linear blocks in the ADC. The non-linear blocks study the behaviour of ADC using experimental analysis.

The optical link that generates some non-ideal behaviour were considered as the DFB laser intensity noise. The intensity noise are due to attenuation, chromatic, dispersion, shot and thermal noise of the optical fibre and the photo detector.

5. Results and Discussion

The achievement of the proposed is analyzed using MATLAB Simulink tool. The analysis is carried out in the 4×4 MIMO LTE system with 3.2GHz 5G signal having 64-QAM over 70Km of SSMF. Here, A^2 optimization strategy is introduced to optimize the bias current and power transmission of the MIMO RoF system. However, the MIMO system requires high BW and hence band pass sampling is introduced to minimize the BW in the system. The performance of the proposed work is analysed under conventional A-RoF and D-RoF system.

5.1. Performance metrics

The EVM is the difference between nominal complex value of received signal and demodulated signal. It can measure the signal BW and modulation imperfections more accurately. The spatialMux transmission in MIMO design are always influenced by one another. The performance of the A-RoF and D-RoF are calculated using EVM and it is mathematically formulated as,

$$EVM(\%) = \sqrt{\frac{\frac{1}{N} \sum_{n=1}^N |x_n - x_{0,m}|^2}{\frac{1}{N} \sum_{n=1}^N |x_{0,m}|^2}} \quad (34)$$

Here, x_n indicates the normalization of n -th symbol, $x_{0,m}$ indicates the normalized ideal constellation point in the n -th symbol, N represents the number of unique constellation symbols.

The performance analysis of D-RoF and A-RoF can be examined using eye diagrams for the transmitting signals. The EOP is also known as eye opening amplitude (EOA) is the ratio of non-distorted reference eye to the eye opening for the distorted eye known as eye opening height (EOH). It is mathematically formulated as,

$$EOP(\text{dB}) = 10 \log \left(\frac{EOA}{EOH} \right) \quad (35)$$

SNR is the ratio of signal power to the noise power and its unit is decibel (dB). It is mathematically formulated as,

$$SNR = 10 \log_{10} \left(\frac{P_{\text{signal}}}{P_{\text{noise}}} \right) \quad (36)$$

Here, p_{signal} represents signal power, p_{noise} indicates the noise power.

5.2. Performance analysis of D-RoF and A-RoF system

In this section, the performance of the D-RoF and A-RoF system are analyzed based on EVM, SNR and EOP by varying the input power, fiber length and resolution bits. From the graph, it clearly illustrates that the proposed A-RoF and D-RoF system shows better performance with low attenuation.

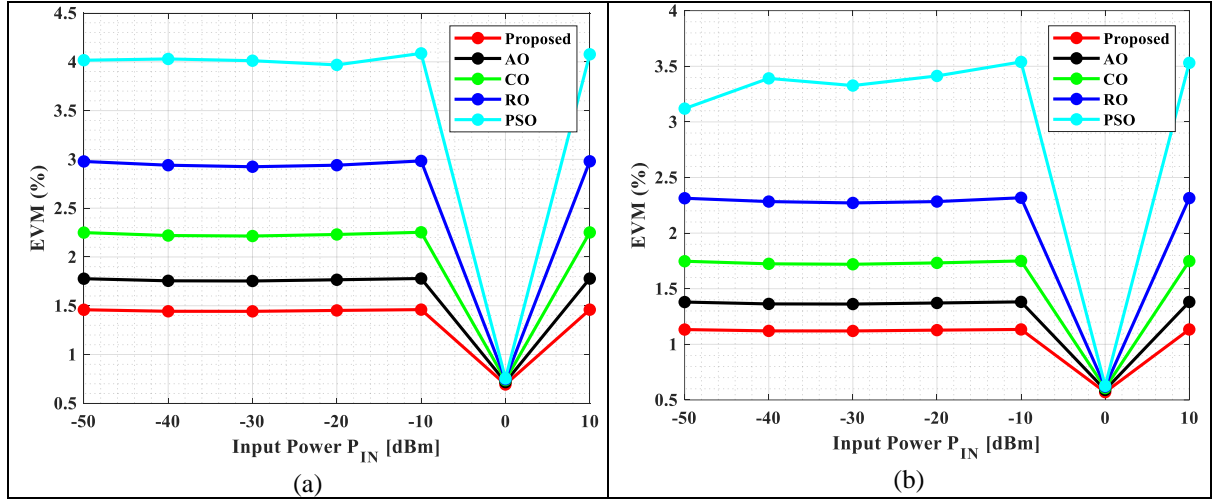


Figure 2: EVM versus input power, (a) EVM performance for A-RoF, (b) EVM performance for D-RoF

Figure (2) illustrates the performance of EVM under varying input power. Figure (2a), (2b) illustrates the EVM performance for A-RoF and D-RoF. From the graph, it is shown that the both system produces the similar outcome for the varying input power. Generally, if the input power gets increased, the EVM gets decreased. Based on the noise power, the signal power gets increased. For A-RoF and D-RoF, the proposed algorithm attains the EVM of 1.45% and 1.13% at 10dBm input power respectively. Due to enhanced PAPR, the modulated signal diminishes the DFB laser to attain below the threshold based on the distortion of optical carrier signal. In D-RoF link, the EVM gets increased when the input power is in 0dBm due to some non-linearity in the ADC system. For the A-RoF link, the dynamic range lies in-between -15dBm and 0dBm. For the D-RoF link, the dynamic range lies in-between -22dBm and 5dBm. For Analog RoF system, dynamic range is chosen in accordance with the 3GPP limit which is almost half than digital RoF. The graphical illustration proves that the received symbol for the D-RoF attains 3GPP of 8% limit under the input power of 5dBm. From the deep analysis of the graph, analog RoF signal produces high noise than digital RoF link under same input power.

Table 1: Comparison of existing methods in terms of EVM for A-RoF

Approaches	EVM performance under A-RoF for varying fiber length						
AO [21]	0.246	0.506	0.767	1.030	1.258	1.525	1.757
CO [22]	0.311	0.640	0.974	1.311	1.591	1.931	2.221
RO [23]	0.410	0.848	1.295	1.750	2.107	2.560	2.940
PSO [24]	0.566	1.175	1.781	2.422	2.963	3.536	3.991
Proposed	0.203	0.415	0.629	0.843	1.034	1.251	1.444

Table 2: Comparison of existing methods in terms of EVM for D-RoF

Approaches	EVM performance under D-RoF for varying fiber length						
AO [21]	0.191	0.393	0.596	0.800	0.977	1.184	1.364
CO [22]	0.241	0.497	0.756	1.018	1.236	1.500	1.725
RO [23]	0.318	0.659	1.00	1.359	1.636	1.988	2.284
PSO [24]	0.490	1.081	1.539	2.095	2.563	3.253	3.100
Proposed	0.158	0.322	0.488	0.655	0.803	0.972	1.121

Initially, the input power P_{IN} is set to 0dBm. The A-RoF curve demonstrates that if the fibre length increase automatically the EVM also gets increased. For the length greater than 60Km, the A-RoF link increases its 3GPP threshold of EVM as 8%. But the D-RoF link preserve the EVM value lower than 3% based on varying length of the RoF link. From the deep analysis of the graph, the 64 bit QAM receive its constellation for both A-RoF and D-RoF link at the length of 70Km. However, the received outcome are more dispersed in case of A-RoF link and confirms that latter is poorly affected by some impairments present in the system. For A-RoF and D-RoF, the proposed algorithm attains the EVM of 1.44%, 1.12% at 70km length respectively. The change in volume for both the system is calculated using EVM by varying the input powers. The graphical illustration proves that the EVM for 0dBm input power attains a value which is more or less than 8% at the length of 70Km. The value attained for both A-RoF and D-RoF is compared with existing techniques such as AO, CO, RO and PSO is illustrated in table (1) and (2) respectively.

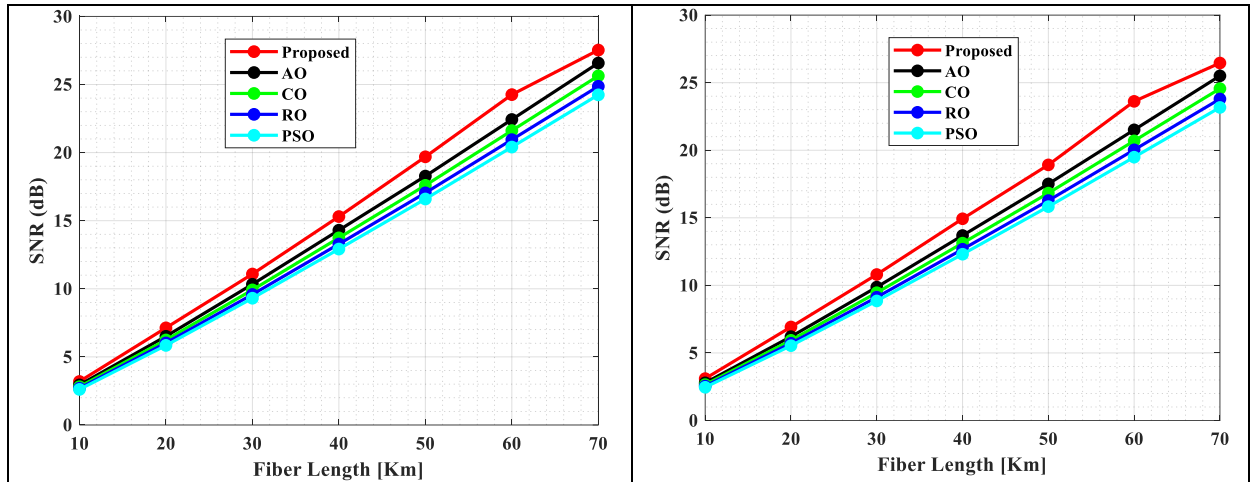


Figure 3: SNR versus fibre length, (a) SNR performance of A-RoF, (b) SNR performance of D-RoF

Figure (3) manipulates the performance of SNR by varying the fibre length. Figure (3a), (3b) illustrates the SNR performance of A-RoF and D-RoF respectively. From the graph, it is shown that the performance of D-RoF is better than A-RoF. It is shown the D-RoF performs better compared to A-RoF approach. From the deep analysis of the graph, as the fiber length also gets increased, the performance of the SNR also gets increased. For the A-RoF and D-RoF, the proposed algorithm attains the EVM of 27dB and 26dB for 70km length respectively. Thus, the quantization noise of the ADC does not affect the SNR value of both the architecture. If the length gets increased, the noise from the optical receiver begin to control the quantization noise. As a result, high fibre loss occurs by limiting the entire link performance. For the A-RoF system, the attenuation of the signal may occur due to continuous degradation of SNR in the RoF link.

Table 3: Comparison of existing methods in terms of EOP for A-RoF

Approaches	EOP performance under A-RoF for varying fiber length						
------------	--	--	--	--	--	--	--

AO [21]	78.846	60.66	62.79	54.23	53.06	50.187	53.351
CO [22]	79.433	68.212	65.81	59.364	56.274	50.97	56.88
RO [23]	82.05	85.078	65.960	60.546	60.213	54.92	60.312
PSO [24]	86.39	92.79	68.8	66.88	60.40	87.49	65.8
Proposed	77.01	49.98	49.56501	49.20	52.67	49.72	51.19

Table 4: Comparison of existing methods in terms of EOP for D-RoF

Approaches	EOP performance under D-RoF for varying fiber length						
AO [21]	66.35	67.95	95.099	57.97	57.63	50.504	58.756
CO [22]	84.436	72.557	98.54	63.87	59.01	51.85	65.76
RO [23]	88.56	75.46	103.89	67.44	70.49	52.244	70.647
PSO [24]	120.65	75.904	124.04	83.802	71.93	58.48	77.67
Proposed	62.56	64.53	74.54	53.992	54.434	48.459	51.051

In case of A-RoF system, the EOH gets closed after the distance of 70Km. Due to this, the EOP attains infinity between the RoF links. In case of D-RoF system, the EOH remains unclosed within the fibre limit (70Km). When the distance is at 70Km, the proposed algorithm attains the EOP almost equal value for A-RoF and D-RoF system respectively. For shorter distance of 10Km, the proposed algorithm attains the EOP of 77dB and 62dB for A-RoF and D-RoF respectively. The performance of EVM and EOP allows to evaluate the quality of the received signal. The value attained for both A-RoF and D-RoF is compared with existing techniques such as AO, CO, RO and PSO is illustrated in table (3) and (4) respectively.

Table 5: Comparison of existing methods in terms of EVM for A-RoF

Approaches	EVM performance under A-RoF for varying fiber length						
AO [21]	1.730	1.782	1.776	1.737	1.796	1.792	1.769
CO [22]	2.181	2.257	2.25	2.18	2.280	2.280	2.24
RO [23]	2.88	2.99	2.98	2.87	3.030	3.05	2.98
PSO [24]	3.93	4.08	4.056	3.96	4.15	4.194	4.11
Proposed	1.425	1.46	1.45	1.43	1.47	1.46	1.4

Table 6: Comparison of existing methods in terms of EVM for D-RoF

Approaches	EVM performance under D-RoF for varying fiber length						
AO [21]	1.343	1.384573	1.379712	1.349121	1.395345	1.392149	1.374323
CO [22]	1.694619	1.753635	1.748448	1.69793	1.771384	1.771241	1.742123
RO [23]	2.239673	2.322372	2.321231	2.230447	2.353972	2.368836	2.317299
PSO [24]	3.129504	3.675342	3.232265	3.607261	3.740284	3.52525	3.457422
Proposed	1.107	1.13608	1.132118	1.112037	1.143156	1.139684	1.127878

The number of bits gets increased, the EVM gets decreased. When the input power is at 0dBm, the fibre is chosen at the length of 70Km. For performing better performance, 8 bit ADC is selected that helps to reduce the EVM more efficiently. When one bit ADC is chosen, the proposed algorithm attains the EVM of 1.4% and 1.10% for both A-RoF and D-RoF respectively. For the 8bit ADC, the proposed algorithm attains the EVM of 1.45% and 1.12% respectively. When the number of bits increased to greater than 8bit, the performance of the EVM does not gets changed. However, the ADC having low bit resolution, high error may attains and the EVM also gets automatically increased. The value attained for both A-RoF and D-RoF is compared with existing techniques such as AO, CO, RO and PSO is illustrated in table (5) and (6) respectively.

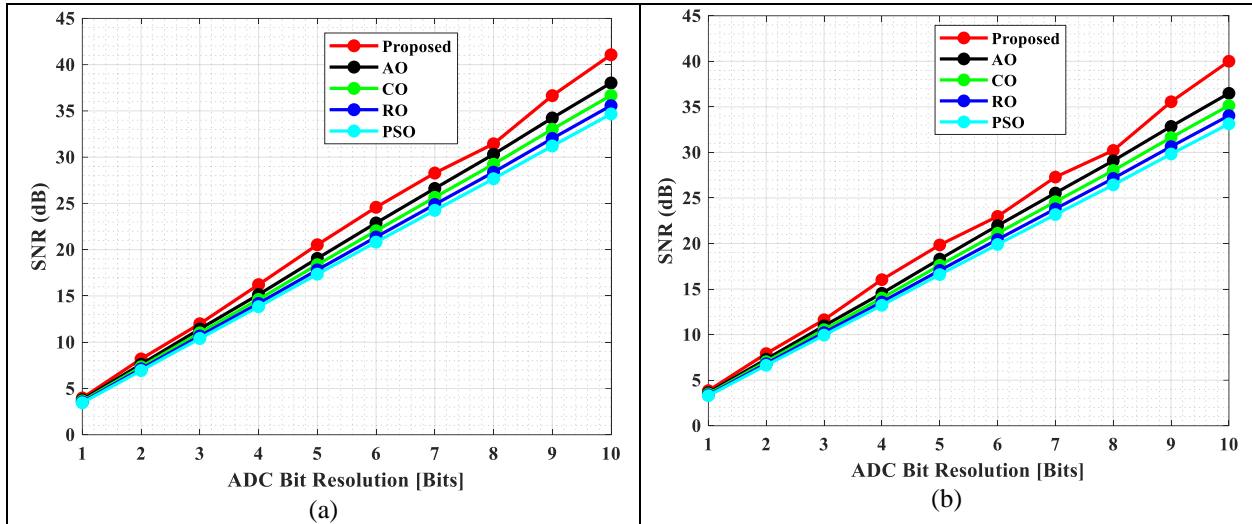


Figure 4: SNR versus ADC bit resolution, (a) SNR performance for A-RoF, (b) SNR performance for D-RoF

Figure (4) illustrates the performance of SNR by varying the number of ADC resolution. Figure (4a) and (4b) depicts the SNR performance of A-RoF and D-RoF respectively. From the graph, as the number of bits gets increased the SNR also gets increased. In one bit ADC, the proposed algorithm attains the SNR of about 3.97dB and 3.85dB for both A-RoF and D-RoF respectively. In 8-bit ADC, the proposed algorithm attains the SNR of about 28dB and 27dB for A-RoF and D-RoF respectively. If the number of bits greater than 8-bit the SNR value does not get changed. From the deep analysis of the graph, it is clear that the selected ADC shows better SNR compared to other ADCs.

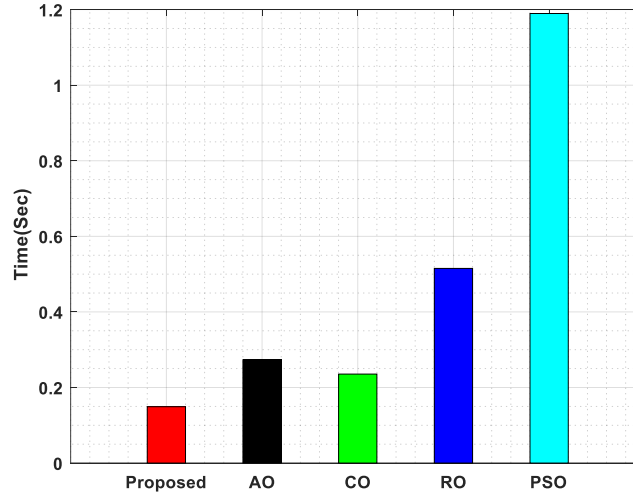


Figure 5: Comparison of overall computation time (sec)

Figure (5) manipulates the comparison of overall computation time (sec). From the deep analysis of the graph, the proposed method attains low computational complexity. Hence, the proposed approach proves the efficiency of the proposed method. The computational performance is compared with other existing techniques such as AO, CO, RO and PSO to prove the performance of the proposed method. The existing AO, CO, RO, PSO and proposed algorithm attains the value of 0.27s, 0.23s, 0.51s, 1.18s and 0.14s respectively. The existing method attains high computational complexity due to in-balance ADC and DAC operation. As the fiber length increases, the performance of the ADC and DAC gets lagged leading to severe traffic among the MIMO system. The proposed method attains low computation time due to the usage of highly enhanced ADC and DAC in the MIMO system.

6. Conclusion

MIMO-LTE RoF link is one of the growing technology in 5G WC system. This research mainly focus to enhance the transmission condition of the RoF Spatial Mux MIMO-LTE System. Here, each antenna deals with 800 MHz 5G signal having 64-QAM over 70Km SSMF is considered to transmit the signal over a distributed applications. However, the MIMO system requires huge BW to transmit the signal over the RoF link. Hence, band pass sampling is introduced. The performance of the proposed method is analysed for both A-RoF and D-RoF systems. Along with this, the transmission condition of the MIMO system is also analysed. In addition to this, A^2 optimization strategy is introduced to optimize the bias current and power transmission in the MIMO RoF system. The performance measures such as EVM, SNR and EOP are analysed under both A-RoF and D-RoF system. In experimental scenario, the A-RoF and D-RoF has the EVM of 1.45% and 1.13%, EOP of 51.19dB and 51dB, SNR of 27dB and 26dB, computation time of 0.14s are attained. The proposed MIMO system are very much useful wireless LAN network for enhancing the network efficiency of the LTE system. The RoF link introduced in this work helps to prevent electromagnetic interference during data transmission. In future, transmission condition can be optimized in a better way using new optimization strategy.

7. References

- [1] S.I. Naqvi, N. Hussain, A. Iqbal, M. Rahman, M. Forsat, S.S. Mirjavadi and Y. Amin, Integrated LTE and millimeter-wave 5G MIMO antenna system for 4G/5G wireless terminals. *Sensors* 20(14) (2020) 3926.
- [2] M.U. Hadi, A. Basit and K. Khurshid, MIMO Enabled MultiBand 5G NR FiberWireless using Sigma Delta over FiberTechnology. In 2021 International Bhurban Conference on Applied Sciences and Technologies (IBCAST), IEEE, (2021) 1007-1010.
- [3] Y-H. Nam, M.S. Rahman, Y. Li, G. Xu, E. Onggosanusi, J. Zhang and J-Y. Seol, Full dimension MIMO for LTE-Advanced and 5G. In 2015 Information Theory and Applications Workshop (ITA), IEEE, (2015) 143-148.
- [4] N. Jaglan, S.D. Gupta and M.S. Sharawi, 18 element massive MIMO/diversity 5G smartphones antenna design for sub-6 GHz LTE bands 42/43 applications. *IEEE Open Journal of Antennas and Propagation* 2 (2021) 533-545.
- [5] N. Chen, B. Rong, X. Zhang and M. Kadoch, Scalable and flexible massive MIMO precoding for 5G H-CRAN. *IEEE Wireless Communications* 24(1) (2017) 46-52.
- [6] E. Ruggeri, A. Tsakyridis, C. Vagionas, G. Kalfas, R.M. Oldenbeuving, P.W.L. van Dijk, C.G.H. Roeloffzen, Y. Leiba, N. Pleros and A. Miliou, A 5G fiber wireless 4Gb/s WDM fronthaul for flexible 360 coverage in V-band massive MIMO small cells. *Journal of Lightwave Technology* 39(4) (2021) 1081-1088.
- [7] G. Femenias, F. Riera-Palou, X. Mestre and J.J. Olmos, Downlink scheduling and resource allocation for 5G MIMO-multicarrier: OFDM vs FBMC/OQAM. *IEEE access* 5 (2017) 13770-13786.
- [8] N. Jaglan, S.D. Gupta, B.K. Kanaujia and M.S. Sharawi, 10 Element Sub-6-GHz Multi-Band Double-T Based MIMO Antenna System for 5G Smartphones. *IEEE Access* 9 (2021) 118662-118672.
- [9] A.S.A. Hassan, Performance Analysis of cell Downlink Throughput For mmWave Massive MIMO 5G (LTE-A Release 15) Network.
- [10] K. Jallouli, A. Hasnaoui, J-P. Diguët, A. Monemi and S. Hasnaoui, Parallel IFFT/FFT for MIMO-OFDM LTE on NoC-Based FPGA. In *International Conference on Advanced Information Networking and Applications*, Springer, Cham, (2022) 542-553.
- [11] S. Rajbhandari, Nonlinear limit of alternative method to 2×2 MIMO for LTE RoF system. *power* 50(4) (2014) 300-301.
- [12] B. Abuhaija, Performance analysis of wireless power harvesting over signal to interference plus noise channel for full-duplex services in LTE MIMO system. *International Journal of Communication Systems* 34(12) (2021) e4892.

- [13] C.H. Nishanthi and N. Ramamurthy, Improving spectral efficiency and low latency in 5G framework utilizing FD-MIMO. *Journal of Ambient Intelligence and Humanized Computing* 12(7) (2021) 6955-6967.
- [14] M.M. Fakharian, A massive MIMO frame antenna with frequency agility and polarization diversity for LTE and 5G applications. *International Journal of RF and Microwave Computer-Aided Engineering* 31(10) (2021) e22823.
- [15] A. Pant, M. Singh and M.S. Parihar, A frequency reconfigurable/switchable MIMO antenna for LTE and early 5G applications. *AEU-International Journal of Electronics and Communications* 131 (2021) 153638.
- [16] C. Mateo, P.L. Carro, P. Garcia-Ducar, J. de Mingo and I. Salinas, Evaluation of Nonlinear Effects in a RoF SpatialMux MIMO-LTE Fronthaul System. In *2018 IEEE 87th Vehicular Technology Conference (VTC Spring)*, (2018) 1-5.
- [17] C. Mateo, P.L. Carro, P. Garcia-Ducar, J. de Mingo and I. Salinas, RoF spatialMux MIMO-LTE fronthaul system transmission parameter selection with nelder-mead optimization algorithm. In *2018 IEEE/MTT-S International Microwave Symposium-IMS, IEEE*, (2018) 1046-1049.
- [18] H. Hafez and A. Mokhtar, Performance Analysis of Transmit Diversity and Spatial Multiplexing MIMO Techniques in LTE Cell Edge Coverage Areas. In *Proceedings of the 2019 8th International Conference on Software and Information Engineering*, (2019) 136-140.
- [19] T. Kanesan, W.P. Ng, Z. Ghassemlooy and C. Lu, Theoretical and experimental design of an alternative system to 2×2 MIMO for LTE over 60 km directly modulated RoF link. In *2012 IEEE Global Communications Conference (GLOBECOM), IEEE*, (2012) 2959-2964.
- [20] J. Kim, M. Sung, S-H. Cho, Y-J. Won, B-C. Lim, S-Y. Pyun, J-K. Lee and J.H. Lee, MIMO-supporting radio-over-fiber system and its application in mmWave-based indoor 5G mobile network. *Journal of Lightwave Technology* 38(1) (2019) 101-111.
- [21] G. Vashishtha and R. Kumar, Autocorrelation energy and aquila optimizer for MED filtering of sound signal to detect bearing defect in Francis turbine. *Measurement Science and Technology* 33(1) (2021) 015006.
- [22] Y. Yang, Y. Wu, H. Yuan, M. Khishe and M. Mohammadi, Nodes clustering and multi-hop routing protocol optimization using hybrid chimp optimization and hunger games search algorithms for sustainable energy efficient underwater wireless sensor networks. *Sustainable Computing: Informatics and Systems* 35 (2022) 100731.
- [23] A. Almalawi, A.I. Khan, F. Alqurashi, Y.B. Abushark, M.M. Alam and S. Qaiyum, Modeling of Remora Optimization with Deep Learning Enabled Heavy Metal Sorption Efficiency Prediction onto Biochar. *Chemosphere* (2022) 135065.
- [24] M.H. Aghdam and A.A. Sharifi, PAPR reduction in OFDM systems: An efficient PTS approach based on particle swarm optimization. *ICT Express* 5(3) (2019) 178-181.